A comparative analysis of compressive sensing approaches for recovery of missing samples in an implantable wireless Doppler device

Ervin Sejdić* Michael A. Rothfuss Michael L. Gimbel† Marlin H. Mickle

Abstract

An implantable wireless Doppler device used in microsurgical free flap surgeries can suffer from lost data points. In order to recover the lost samples, we considered approaches based on recently proposed compressive sensing. In this paper, we carried out a comparative analysis of several different approaches using synthetic signals and real signals obtained during blood flow monitoring in four pigs. We considered three different basis functions: Fourier basis, discrete prolate spheroidal sequences and modulated discrete prolate spheroidal sequences. To avoid the computational burden, we considered approaches based on the l_1 minimization for all three bases. To understand the trade-off between the computational complexity and the accuracy, we also used a recovery process based on matching pursuit and modulated discrete prolate spheroidal sequences bases. For both synthetic and real signals, the matching approach with modulated discrete prolate spheroidal sequences provided the most accurate results. Future studies should focus on the optimization of the modulated discrete prolate spheroidal sequences in order to further decrease the computational complexity and increase the accuracy.

Keywords: Signal reconstruction, compressive sensing, wireless Doppler, modulated discrete prolate spheroidal sequences, time-frequency dictionary, matching pursuit.

*Ervin Sejdić, Michael A. Rothfuss and Marlin H. Mickle are with the Department of Electrical and Computer Engineering, Swanson School of Enginering, University of Pittsburgh, Pittsburgh, PA, USA. E-mails: esejdic@ieee.org, mar28@pitt.edu, mickle@pitt.edu.

†Michael L. Gimbel is with the Department of Plastic Surgery, University of Pittsburgh, Pittsburgh, PA, USA. E-mail: gimbelml@upmc.edu.

1 Introduction

In microsurgical free flaps (MFF), large blocks of tissue (flaps) are borrowed from one part of a patient's body (e.g., abdominal skin/fat, bone, etc) and are used to reconstruct major defects in another part of the body (e.g. breast, mandible, etc) [1], [2], [3]. These procedures require connecting tiny blood vessels to allow blood flow [4], [5]. Hence, successful MFF reconstructive procedures depend upon uninterrupted blood flow. Unfortunately, blood flow is compromised in approximately 10% of cases in the first several days after surgery [6], [7], [8]. In these events, prompt re-operation to correct the problem is paramount. For this reason, surgeons and nurses monitor blood flow very frequently in the first few postoperative days using blood flow monitoring devices [9], [10]. However, the gold standard of blood flow monitoring systems suffer from unreliability and a high (up to 30%) false positive rate (i.e., the device signals a problem when none exists, leading to unnecessary and morbid reoperation), both problems largely due to the device's design which features a cumbersome and easily dislodged wire that exits through the patient's skin [11], [12], [13]. Because the wire that exits through the patient's skin is chiefly responsible for the unreliability and false positives associated with monitoring the flap [14], a natural solution to this problem is to eliminate the wire.

Our team has been developing an implantable wireless Doppler blood flow monitor. The advantage of our system is that the entirety of the monitoring device is implanted with no wires protruding through the patient's skin. The digitized Doppler flow signals on the implantable device are transmitted wirelessly from inside the body to an external radio receiver. The radio receiver converts the wireless radio frequency signals into digital baseband. The digital baseband at the external radio receiver is transmitted via USB to a laptop computer, where the digital data is stored on the hard disk drive. On the laptop, the digital data are converted and processed to display the time-domain blood flow signals in audio baseband. Additionally, the audio baseband is sent to speakers for audible confirmation of flow.

If data are lost or corrupted due to poor wireless reception the loss is simply ignored; therefore, no re-transmission requests are sent from the radio receiver to the implanted transmitter. The lost or corrupted data can result from a number of sources including: multipath fading, low signal-to-noise ratio, adjacent channel interferers, [15], [16]. The multipath fading problem manifests as copies of the transmitted signal, which arrive at the receiver at different times due to the signal reflecting from objects in the environment (e.g., chairs, walls, floor, ceiling, humans, etc.). The time-delayed copies of the transmitted signal add in time to produce constructive and destructive interference

and inter-symbol interference. If the signal arriving at the receiver is too weak (i.e., below the sensitivity threshold of the receiver for given configuration or buried in noise), then the receiver will be unable to demodulate the transmitted signal. Lost symbols due to variations in the wireless signals' amplitude gain at the receiver antenna follow a Rician distribution according to the Rician fading model for radio signal propagation, and the interval regularity/irregularity of lost symbols is commensurate with the amplitude gain's characteristic Rician distribution. Furthermore, strong adjacent channel interferers (e.g., cell phones) near the operational channel of the implantable radio transmitter and external receiver can desensitize the receiver due to non-linear gain compression if the adjacent channel interferer is not attenuated (e.g., filtered) sufficiently before processing the received radio signal.

The cyclic redundancy check (CRC) used in the current device embodiment served as a quick way to filter erroneous data from correct data when displaying the real-time blood flow information. Future embodiments could insert a parity bit into one of the don't-care bit positions of the memory where the 10-bit ADC samples (i.e., 10-bits occupy two bytes in memory, which means there are six don't-care bits where a parity bit could be inserted) reside, and where the parity bit is computed over the ADC sample's data bits. An approach like this allows for error detection of individual samples in a packet without increasing the amount of transmitted wireless data.

In order to recover missing points, we propose to reconstruct the acquired data based on recently proposed compressive sampling (CS) approaches. While CS is usually used to acquire data in a compressive manner, we utilize these CS approaches to recover missing samples. However, when recovering the missing samples, one needs to choose a domain (i.e., basis functions) that will provide a sparse representation of signals. In this paper, we carry out a comparative analysis using three different choices: Fourier basis, discrete prolate spheroidal sequences (DPSS) and modulated discrete prolate spheroidal sequences (MDPSS) [17], [18]. MDPSS are obtained by modulation and variation of the bandwidth of DPSS to reflect the varying time-frequency nature of blood flow signals. Using the considered approaches, we carried out a numerical analysis of synthetic test signals and real blood flow Doppler signals. The numerical analysis using the synthetic test signals showed that the recovery of the signals based on MDPSS was more accurate than the Fourier basis or DPSS (e.g., [19], [20]).

The paper is organized as follows: Section 2 describes the wireless Doppler system that our team has developed. In Section 3, we described the data collection approach. Section 4 reports the data analysis steps that we carried out to obtain the reported results, which are presented in Section 5 along with the discussion of the same results. The conclusions are drawn in Section 6.

2 A system for wireless Doppler monitoring of blood flow

Figure 1 shows the developed implantable wireless Doppler device. The device comprises custom-designed circuitry for sensing, digitizing, and wirelessly transmitting Doppler-shifted signals, and a cylindrical cuff inset with piezoelectric ultrasonic transducers in a continuous-wave Doppler configuration, which is affixed to the vessel under test (VUT) for the experiments. The Doppler-shifted electrical signals are generated by the scattering effect of particles (e.g., red blood cells) in flowing blood in the presence of an insonating ultrasonic acoustic wave. The Doppler-shifted acoustic wave is converted to an electrical signal by a piezoelectric transducer. The Doppler-shifted electrical signal is conditioned and converted to audio baseband in hardware before digitization by a 10-bit ADC.

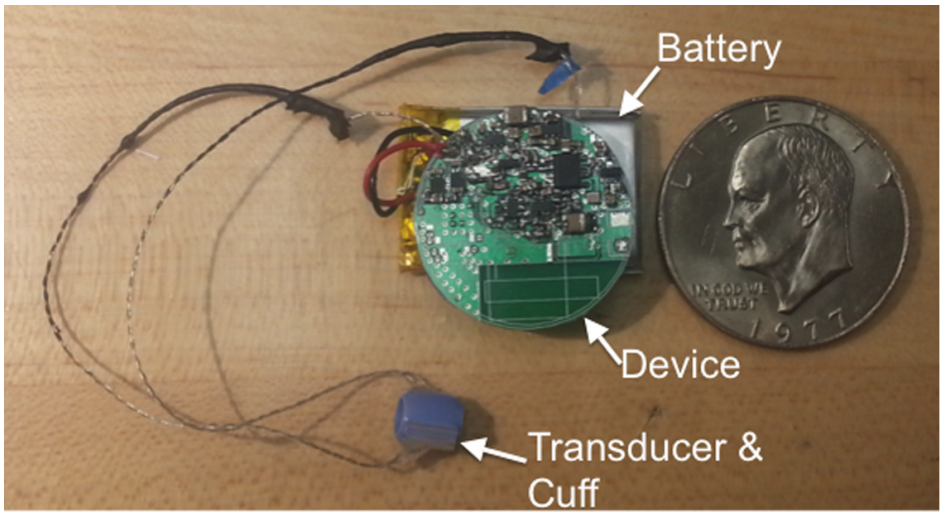

Figure 1: The wireless implantable Doppler device used in the experiments.

All data processing (i.e., analog and digital) and wireless transmissions were performed sufficiently quick to maintain a real-time system. A real-time system allowed quick assessment of the physiological changes in blood flow during the experiments. The digitized Doppler signals were transmitted wirelessly via the implantable device's radio electronics. The digitized time-domain blood flow signal data at the implantable device aggregates in the radio transmitter's memory until a sufficiently large quantity of data samples are collected. This sufficient quantity of aggregated digital data are transmitted wirelessly as a packet, and each packet is packed with two identifiers (i.e., a sequence number and a cyclic redundancy check). A cyclic redundancy check is used to check if the received packet is corrupted, and a sequence number in a packet is a simple numer-

ical signature intended to assist in checking for missing packets. These two identifiers assist the post signal processing performed on the stored data, in that groups of sequential packets can be identified. A wireless radio receiver converted the over-air wireless data, sent from the implanted device, to digital data. Lost wireless data (i.e., missed or corrupted data packets at the receiver) were ignored to facilitate the real-time nature of the system.

CRC-16 was used to detect corrupted data in a received packet [21]. Before the implantable device's radio transmits a packet, the CRC was computed over the data payload (i.e., ADC samples and any additional packet data such as a packet sequence number), and then the CRC-16 checksum was appended to the packet for wireless transmission [22]. At the external radio receiver, a new CRC was computed over the received data payload, and it is matched to the aforementioned appended CRC-16 checksum [23]. If the new CRC-16 checksum matched the appended CRC-16 checksum, then the packet was assumed to have been received without error. If the checksums do not match, then the packet was assumed to have been received with error, and thus, the packet was ignored.

All received digital data were sent over a serial communication bus to a hardware serial-to-Universal Serial Bus (USB) converter. The serial-to-USB converter buffers and converts the serial data to the USB protocol for transmission to a laptop's USB port. The laptop's USB port was configured to emulate a serial port; in essence, the serial data coming out of the external receiver passes through to the computer's internal buffer memory using the serial-to-USB converter and USB-to-serial emulator.

A computer software program was designed to read the computer's internal buffer memory, and these read data are subsequently stored on the computer's hard disk drive in a file. The read data are also processed such that it can be visually displayed on the computer's screen (i.e., time-domain audio baseband signals) in real-time. Furthermore, this same audio baseband information is also sent to computer speakers for clinical observation.

3 Data collection

The protocol for the study was approved by the Institutional Animal Care and Use Committee at the University of Pittsburgh. Four pigs were used for the experiments, and 32 data sets were collected in total. Data were collected with the Doppler transducer cuff affixed to the femoral vein, and four data sets were collected from each (e.g., right-side and left-side) hind leg of the pigs (i.e., eight data collections from each of the four animals). Figure 2 shows one of the pigs with the implantable Doppler devices connected to the pig's femoral vein.

Each data set was collected as follows: 1.) collect data from the VUT for at least one minute, 2.) occlude the femoral vein proximal to the Doppler transducer cuff, 3.) collect data for at least one minute from the currently occluded vessel, and 4.) remove occlusion placed during step two and collect data for at least one minute.

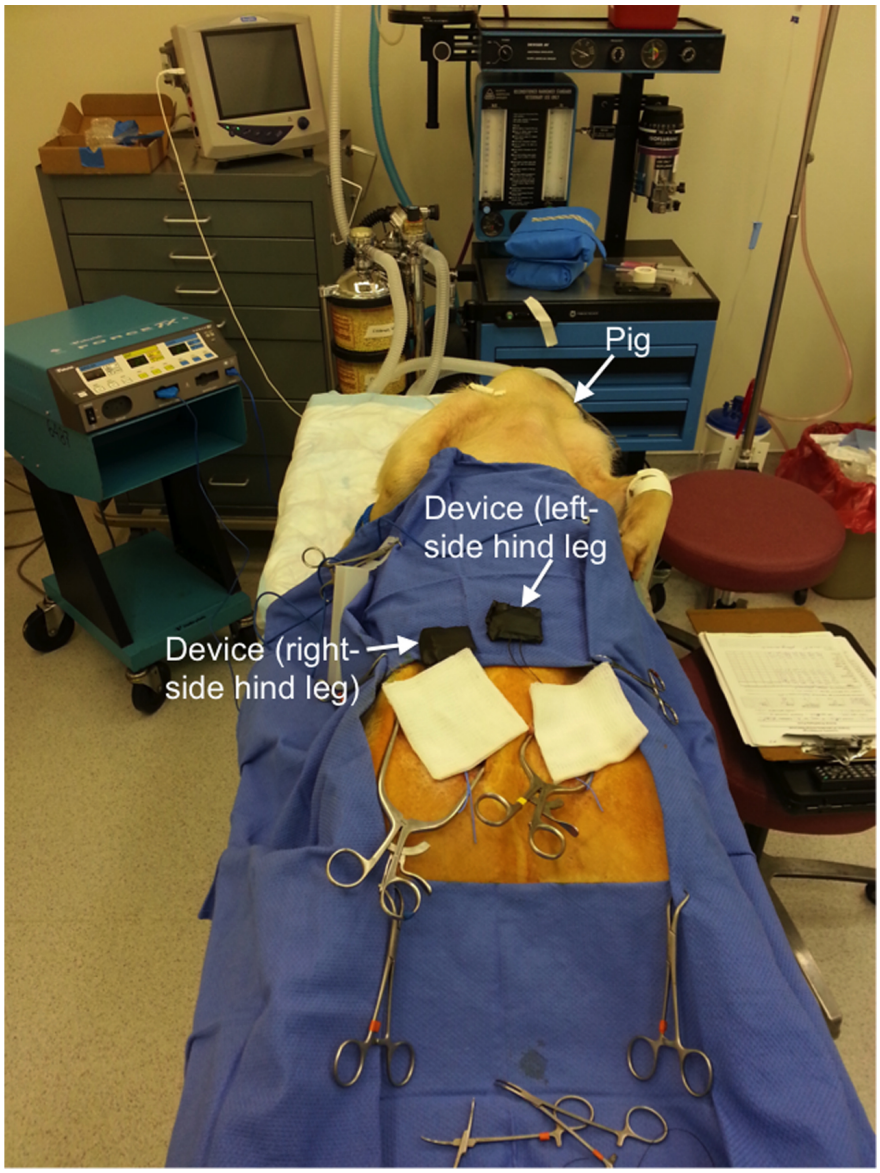

Figure 2: A pig with two wireless implantable Doppler devices attached to the animal's femoral vein. The devices are shown here outside of the body for illustration. The devices are shown encapsulated, which provides a moisture barrier for the electronics during implantation.

4 Recovery of missing samples based on compressive sensing

Compressive sensing (CS) is a method closely related to transform coding, since a transform code converts input signals, embedded in a high-dimensional space, into signals that lie in a space of significantly smaller dimensions (e.g., wavelet and Fourier transforms) [24], [25], [26]. CS approaches are particularly suited for K-sparse signals, i.e., signals that can be represented by significant K coefficients over an N-dimensional basis. Encoding of a K-sparse, discrete-time signal of dimension N is accomplished by computing a measurement vector y that consists of $M << N$ linear projections of the vector s. This can be compactly described via

$$y = \Phi s \tag{1}$$

where Φ represents an $M \times N$ matrix and is often referred to as the sensing matrix [24]. A natural formulation of the recovery problem is within a norm minimization framework, which seeks a solution to the problem

$$\min ||s||_0 \text{ subject to } \|y - \Phi s\|_2 < \eta \tag{2}$$

where η is the expected noise of measurements, $||s||_0$ counts the number of nonzero entries of x and $\|\bullet\|_2$ is the Euclidian norm.

Given the CS framework, the immediate question is how to define the sensing matrix Φ, that is the bases used in the recovery of the signal. Most commonly used sensing matrices are random matrices with independent identically distributed (i.i.d.) entries formed by sampling either a Gaussian distribution or a symmetric Bernoulli distribution [27]. Previous publications have shown that these matrices can recover the signal with high probability [27].

4.1 Data analysis

Our data analysis consists of two parts. In the first part, we consider the synthetic test signals in order to examine the accuracy of the scheme in well-known conditions. In the second part, we use Doppler blood flow signals to examine how accurately we can recover these signals from sparse samples.

However, when dealing with biomedical signals, we would like to "precisely" recover the signals (i.e., with a very small error). Hence, we need to choose an appropriate domain in which these biomedical signals are sparse. If we rewrite eqn. (1) to accommodate this idea, we then obtain [28]:

$$y = \Phi s = \Phi \Psi x \tag{3}$$

where $s = \Psi x$ represents a sparse representation of a biomedical signal in a domain given by Ψ and x represents expansion coefficients. There are a number of different choices for the matrix Ψ. Here, we consider matrices based on Fourier basis, DPSS and MDPSS. Similarly, the minimization given by eqn. (2) is not suitable for many applications as it is NP-hard [29]. To avoid the computational burden, we considered approaches based on the l_1 minimization (e.g., [30], [31]) for all basis matrices:

$$\min ||x||_{\ell_1} \text{ subject to } y = \Phi\Psi x \tag{4}$$

To understand the trade off between the computational complexity and the accuracy, we also used a recovery process based on matching pursuit and MDPSS bases [18], [32], [33].

In order to establish statistical significance of our results, a non-parametric inferential statistical method known as the Mann-Whitney test was used [34], which assesses whether observed samples are drawn from a single population (i.e., the null hypothesis). For multi-group testing, the extension of the Mann-Whitney test known as the Kruskal-Wallis was used [35]. A 5% significance was used.

4.1.1 Synthetic Test Signals

To analyze the proposed scheme, we assumed the following test signal [36]:

$$s(t) = \sum_{i=1}^{M} a_i \cos(2\pi f_i t + \phi_i) \tag{5}$$

where $0 \leq t < 1$ and

$$f_i = (i - 0.5)\Delta f \tag{6}$$

with

$$a_i = \sqrt{2S_s(t, f_i)\nu\Delta f}. \tag{7}$$

$S_x(t, f_i)$ is the time-varying power spectral density defined over the range $f \in [0, f_{\max}]$ and $\Delta f = f_{\max}/M$. $S_x(t, f_i)$ is calculated according to the procedure for continuous wave Doppler signals outlined in [36]. ϕ_i is a random variable uniformly disturbed $[0, 2\pi]$ and ν is a χ^2 random variable with two degrees of freedom. The assumed sampling frequency in this case was $f_s = 16340$ Hz and $f_{\max} = 2500$ Hz.

To emulate the real-life conditions, we assumed that the data were transmitted in the blocks of $N = 256$ samples. The first experiment consisted of maintaining a certain percentage of samples equally spaced throughout the signal. In the second experiment, it was assumed that the samples were irregularly dropped. For both experiments, we assumed that we have between 30% and 90% of

available samples. The lower boundary of 30% samples denotes very poor transmission conditions, where majority of the samples are dropped. On the other hand, the upper boundary of 90% samples represents a realistic case in the operating room. The normalized half-bandwidth W for the DPSS and MDPSS approaches is assumed to be $W = 0.495$. The Fourier basis are generated using the considered N value. Therefore, if s is a $N \times 1$ vector, the values of x are then obtained as:

$$s_{MDPSS} = \left[(\Psi_{MDPSS}\Psi'_{MDPSS})^{-1}\Psi_{MDPSS}\right] x \tag{8}$$

$$s_{DPSS} = \left[(\Psi_{DPSS}\Psi'_{DPSS})\Psi_{DPSS}\right] x \tag{9}$$

$$s_F = \Psi_F x \tag{10}$$

where Ψ_{MDPSS}, Ψ_{DPSS} and Ψ_F represent matrices containing MDPSS, DPSS and Fourier basis functions, respectively. Ψ_{MDPSS} is a $N \times Q$ matrix, and $Q \gg N$ as Ψ_{MDPSS} represents a redundant set of basis functions. The Q value depends on the normalized half-bandwidth W value and the number of modulation bands. Ψ_{DPSS} is an $N \times R$ matrix, and $R = \lfloor 2WN \rfloor$. Ψ_F is an $N \times N$ matrix.

To evaluate the effectiveness of the proposed approach when considering Doppler blood flow signals, we adopted performance metrics used in other biomedical applications (e.g., [26], [37], [38]). Those metrics are:

- A normalized error similarly to the percent root difference measures distortion in reconstructed biomedical signals, and is defined as:

$$NE = \frac{\|s(n) - \widehat{s}(n)\|_2^2}{\|s(n)\|_2^2} \tag{11}$$

  where $s(n)$ is a realization of the signal in a block of length N and $\widehat{s}(n)$ represents a recovered signal.

- Root mean square error (RMSE) - RMSE also measures distortion and is often beneficial to minimize this metric when finding the optimal approximation of the signal. RMSE is defined as:

$$RMSE = \sqrt{\frac{\sum_{n=1}^{N}\left(s(n) - \widehat{s}(n)\right)^2}{N}} \tag{12}$$

- Cross-correlation (CC) - CC is used to evaluate the similarity between the original and the reconstructed signal, and is defined as:

$$CC = \frac{\sum_{n=1}^{N}\left(s(n) - \mu_s\right)\left(\widehat{s}(n) - \mu_{\widehat{s}}\right)}{\sqrt{\sum_{n=1}^{N}\left(s(n) - \mu_s\right)^2}\sqrt{\sum_{n=1}^{N}\left(\widehat{s}(n) - \mu_{\widehat{s}}\right)^2}} \times 100\% \tag{13}$$

where $s(n)$ is the original signal and $\widehat{s}(n)$ represents a reconstructed signal. In addition, μ_s and $\mu_{\widehat{s}}$ denote the mean values of $s(n)$ and $\widehat{s}(n)$, respectively.

- Maximum error (MAXERR) - MAXERR is used to understand the local distortions in the reconstructed signal, and it particularly denotes the largest error between the samples of the original signal and the reconstructed signal. The metric is defined as:

$$MAXERR = \max\left(s(n) - \widehat{s}(n)\right) \tag{14}$$

4.1.2 Blood flow signals obtained via a wireless Doppler device

The considered CS schemes were using to recover missing samples from the blood flow signals. The same experimental procedures are repeated for the these signals as for the synthetic signals. However, we only considered that 65% or 95% of the original samples were available. As illustrative examples, we only considered one second of data from each trial. This provided us with 63 blocks of 256 data samples.

5 Results and Discussion

In this section, we present the results of numerical experiments and discuss those results. First, we will discuss the results based on the synthetic test signals. In the second part, we will discuss the results of numerical experiments considering Doppler blood flow signals.

5.1 Synthetic test signals

Figure 3 depicts the results for synthetic signals when reduced sampling rate was used at regular intervals. These results clearly depict that the CS approaches based on the MDPSS dictionary provided superior performance. It was interesting to note that even a matching pursuit based approach with the MDPSS dictionary provided more accurate results than the l_1 approaches. This is significant as the matching pursuit approach is computationally less demanding than the l_1 approaches. The second major observation was the fact that DPSS based approaches could not achieve accurate recovery even when a high number of samples is used (e.g., more than 70% of samples). All results are statistically different ($p \ll 0.01$).

The results of the simulation using irregular sampling periods are summarized in Figure 4. As in the first simulation, the approach based on DPSS bases cannot provide accurate representations of the simulated signals. The best results are still obtained with the MDPSS matching pursuit

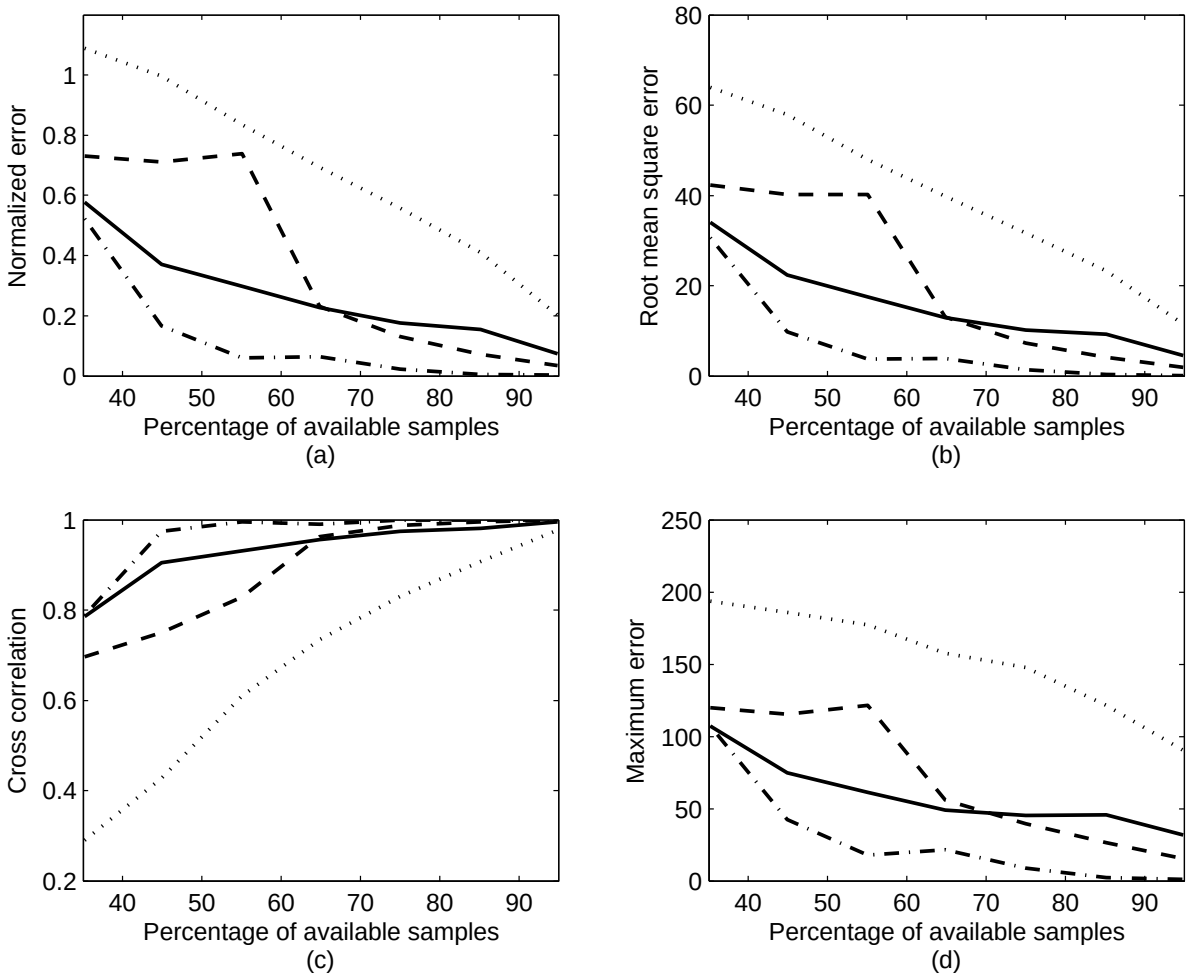

Figure 3: The results for synthetic signals while using regular sampling rates (a) normalized error; (b) root mean square error; (c) cross correlation; and (d) maximum error. The dashed line denotes the results obtained with the Fourier basis; the dotted line indicates the results obtained with the DPSS bases; the dash-dotted line indicates the results obtained with a 25-band MDPSS-based dictionary with matching pursuit; and the solid line indicates the results obtained with a 25-band MDPSS-based dictionary with the l_1 approach.

approach, while the Fourier l_1 approach is the second most accurate approach. It should be mentioned that the results of the second simulation are worse than for the first simulation, which is expected due to the irregular samples. The presented results are statistically different ($p \ll 0.01$).

The presented results clearly show that the approaches based on the Fourier basis and the MDPSS dictionary yield the most accurate results. However, to understand the advantage of the

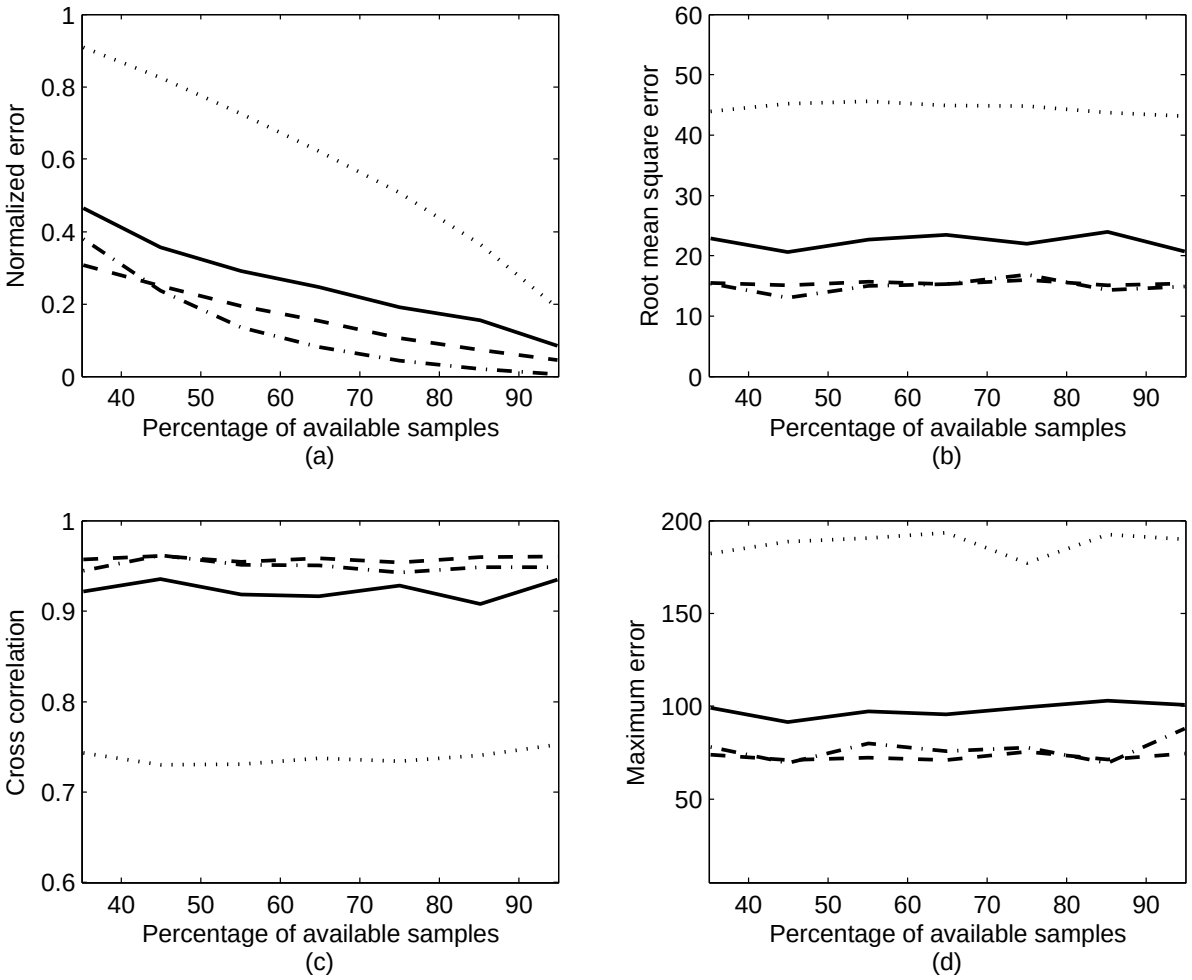

Figure 4: The results for synthetic signals while using irregular sampling rates (a) normalized error; (b) root mean square error; (c) cross correlation; and (d) maximum error. The dashed line denotes the results obtained with the Fourier basis; the dotted line indicates the results obtained with the DPSS bases; the dash-dotted line indicates the results obtained with a 25-band MDPSS-based dictionary with matching pursuit; and the solid line indicates the results obtained with a 25-band MDPSS-based dictionary with the l_1 approach.

approach based on the MDPSS dictionary, let us consider sample error signals (i.e., the differences between the original signal and the reconstructed signal). Figure 5 depicts the analysis using a block of 256 samples. We reconstructed signals while a variable number of samples was available (from 45% to 75% of samples). It was also assumed that the irregular samples were used. It is clear that the error obtain with the MDPSS dictionary is negligible in comparison to the error obtained

with the Fourier basis.

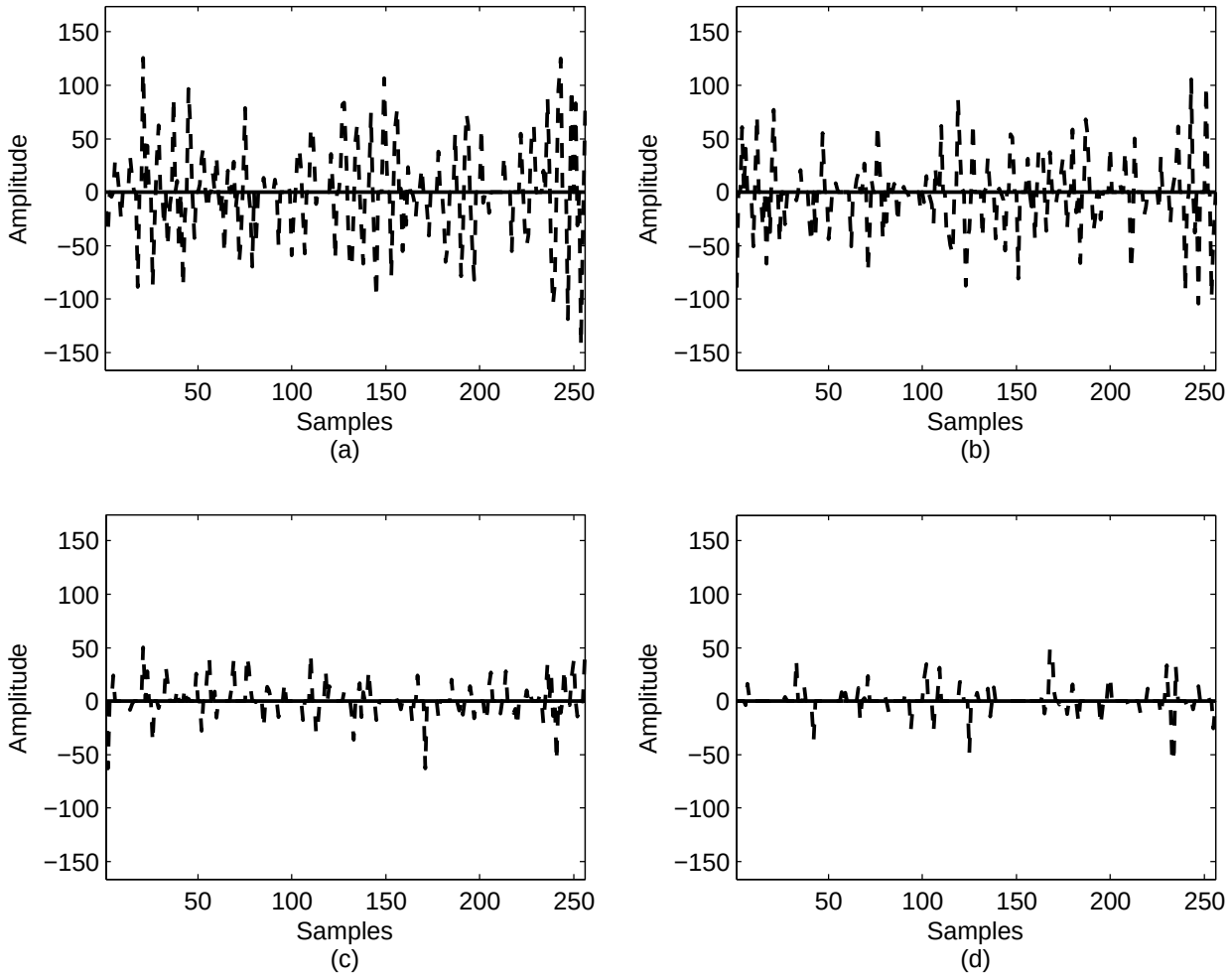

Figure 5: A comparative analysis of sample error signals obtained for the approaches based on Fourier bases and the MDPSS dictionary: (a) 45% of samples available; (b) 55% of samples available; (c) 65% of samples available; (d) 75% of samples available. The dashed line denotes the results obtained with the Fourier basis; the dotted line indicates the results obtained with 25-band MDPSS-based dictionary with matching pursuit.

5.2 Reconstruction of blood flow Doppler signals

Tables 1-4 summarize the results of the numerical analysis when considering one-second samples obtained during the animal trials. Sample signals are shown in Figure 6.

Based on the presented results, we can state that the results obtained with the MDPSS-based

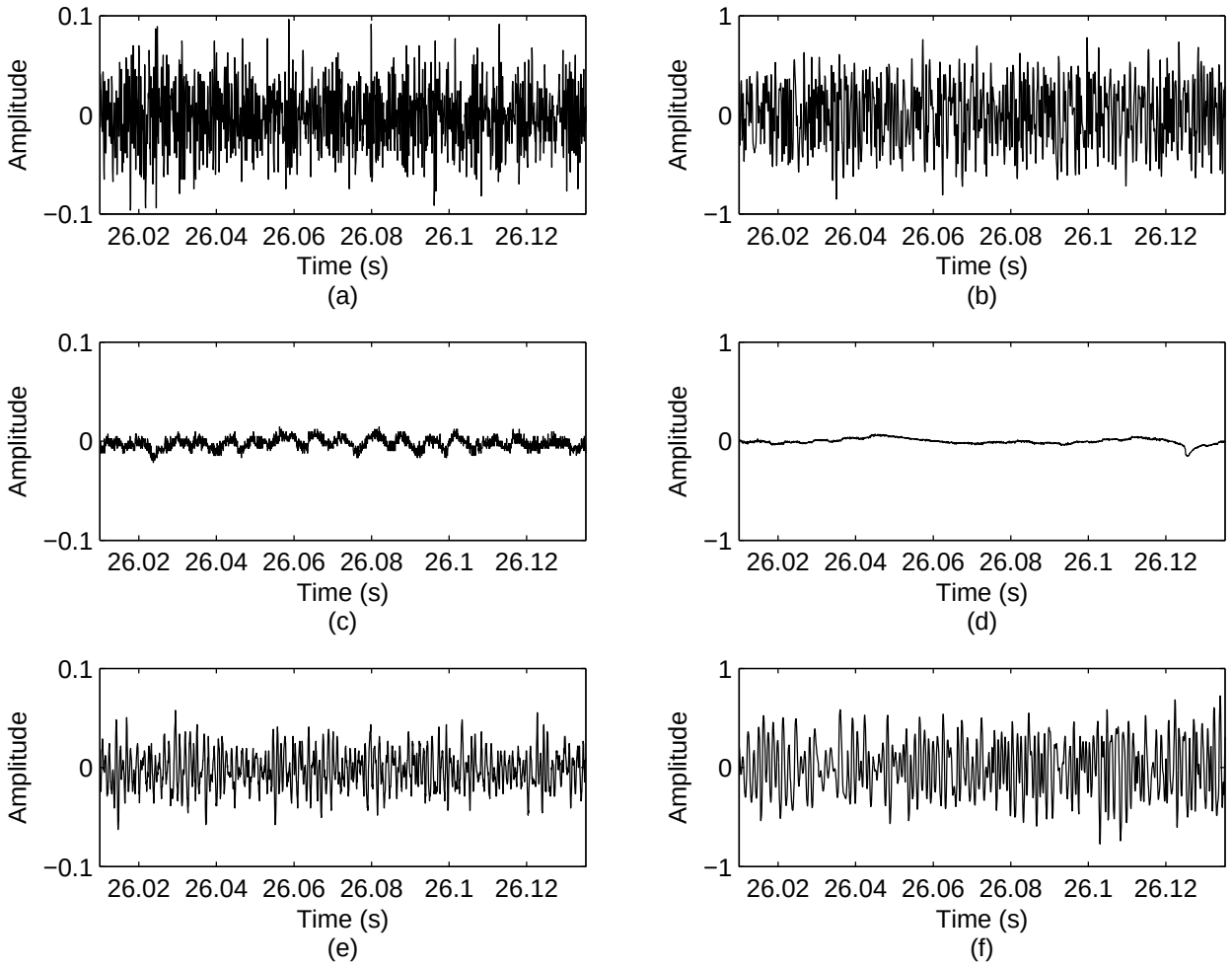

Figure 6: Sample signals obtained from animals: (a) a sample signal in the left leg during first non-occluded recording; (b) a sample signal in the right leg during first non-occluded recording; (c) a sample signal in the left leg during occluded recording; (d) a sample signal in the right leg during occluded recording; (e) a sample signal in the left leg during second non-occluded recording; and (f) a sample signal in the right leg during second non-occluded recording.

matching pursuit and the results obtained with the l_1 minimization are statistically different. In all considered cases, the MDPSS-based matching pursuit outperformed the recovery process based on the Fourier basis and the l_1 minimization. On average, we obtained 30%-40% improvements with the MDPSS approach.

The second major observations was that statistically the results were not affected if the samples were lost in random or uniform manners ($p > 0.19$). This could be explained by the fact that both

of the schemes are very accurate given a high number of available samples. Possible statistical differences may arise if the number of available samples is rather small (e.g., 20%-30% of samples).

Table 1: Performance of the proposed method for recovery of blood flow Doppler signals when considering uniformly missing samples with 65% of samples available. † = multiplication by 10^{-2}. ♯ = statistically different from the MDPSS matching pursuit.

	Flow 1		Occlusion		Flow 2	
Metric	l_1 min	MP	l_1 min	MP	l_1 min	MP
NE	$0.48 \pm 0.18^{\sharp}$	0.33 ± 0.22	$0.41 \pm 0.12^{\sharp}$	0.29 ± 0.15	$0.46 \pm 0.16^{\sharp}$	0.30 ± 0.21
RMSE†	$4.12 \pm 4.64^{\sharp}$	2.35 ± 2.50	$0.79 \pm 1.17^{\sharp}$	0.31 ± 0.14	$4.36 \pm 8.09^{\sharp}$	2.52 ± 5.22
CC (%)	$86.9 \pm 9.19^{\sharp}$	92.3 ± 8.46	$90.1 \pm 5.08^{\sharp}$	94.7 ± 4.00	$87.9 \pm 8.00^{\sharp}$	93.1 ± 8.22
MAXERR	0.33 ± 0.38	0.25 ± 0.30	$0.12 \pm 0.24^{\sharp}$	0.03 ± 0.04	0.38 ± 0.72	0.26 ± 0.48

Table 2: Performance of the proposed method for recovery of blood flow Doppler signals when considering uniformly missing samples with 95% of samples available. † = multiplication by 10^{-2}.

	Flow 1		Occlusion		Flow 2	
Metric	l_1 min	MP	l_1 min	MP	l_1 min	MP
NE	$0.13 \pm 0.07^{\sharp}$	0.09 ± 0.07	$0.16 \pm 0.07^{\sharp}$	0.12 ± 0.06	$0.13 \pm 0.08^{\sharp}$	0.09 ± 0.07
RMSE†	0.95 ± 0.98	0.64 ± 0.64	$0.21 \pm 0.16^{\sharp}$	0.13 ± 0.05	0.99 ± 1.81	0.67 ± 1.31
CC (%)	$98.9 \pm 1.31^{\sharp}$	99.3 ± 0.90	$98.6 \pm 1.09^{\sharp}$	99.1 ± 0.68	$98.9 \pm 1.49^{\sharp}$	99.4 ± 0.99
MAXERR	0.21 ± 0.26	0.17 ± 0.20	$0.05 \pm 0.07^{\sharp}$	0.02 ± 0.01	0.18 ± 0.28	0.16 ± 0.25

The lowest errors were obtained during the occlusion periods. This is expected as signals have a less complex composition during these evens (e.g., compare Figures 6(c) and 6(d) with the other subgraphs). Our findings indicate that it is possible to accurately model the Doppler signals during occlusions, which can potentially diminish the number of false positives even when many samples are lost during the transmission process.

Therefore, the presented results warrant us to state that missing samples can be accurately recovered using the MDPSS bases along with matching pursuit. Further improvements can be obtained by optimizing the characteristics of the MDPSS dictionary such as the level of bands and the initial normalized bandwidth.

Table 3: Performance of the proposed method for recovery of blood flow Doppler signals when considering non-uniformly missing samples with 65% of samples available. † = multiplication by 10^{-2}.

	Flow 1		Occlusion		Flow 2	
Metric	l_1 min	MP	l_1 min	MP	l_1 min	MP
NE	$0.51 \pm 0.17^{\sharp}$	0.38 ± 0.20	$0.41 \pm 0.14^{\sharp}$	0.31 ± 0.14	$0.48 \pm 0.15^{\sharp}$	0.35 ± 0.19
RMSE†	4.45 ± 5.10	3.09 ± 3.50	$0.72 \pm 0.95^{\sharp}$	0.48 ± 0.90	4.21 ± 7.05	2.98 ± 5.34
CC (%)	$85.6 \pm 9.25^{\sharp}$	90.4 ± 8.64	$90.8 \pm 5.66^{\sharp}$	94.3 ± 4.17	$87.3 \pm 8.09^{\sharp}$	91.9 ± 7.87
MAXERR	0.35 ± 0.41	0.32 ± 0.40	0.09 ± 0.16	0.17 ± 0.64	0.34 ± 0.54	0.35 ± 0.54

Table 4: Performance of the proposed method for recovery of blood flow Doppler signals when considering non-uniformly missing samples with 95% of samples available. † = multiplication by 10^{-2}.

	Flow 1		Occlusion		Flow 2	
Metric	l_1 min	MP	l_1 min	MP	l_1 min	MP
NE	$0.14 \pm 0.08^{\sharp}$	0.10 ± 0.07	$0.16 \pm 0.07^{\sharp}$	0.11 ± 0.06	$0.14 \pm 0.08^{\sharp}$	0.09 ± 0.07
RMSE†	1.13 ± 1.19	0.70 ± 0.72	$0.23 \pm 0.21^{\sharp}$	0.13 ± 0.06	1.14 ± 2.02	0.70 ± 1.33
CC (%)	$98.6 \pm 1.59^{\sharp}$	99.3 ± 0.91	$98.4 \pm 1.13^{\sharp}$	99.1 ± 0.66	$98.6 \pm 1.65^{\sharp}$	99.3 ± 0.99
MAXERR	0.23 ± 0.27	0.17 ± 0.21	$0.05 \pm 0.07^{\sharp}$	0.02 ± 0.02	0.23 ± 0.38	0.18 ± 0.33

6 Conclusion

In this paper, we carried out a comparative analysis of compressive sensing algorithms for accurate reconstruction of Doppler blood flow signals. We considered both the synthetic signals and the real Doppler blood flow signals obtained from four animals. In both cases, the MDPSS-based matching pursuit outperformed the l_1 minimization approaches regardless whether orthogonal or redundant basis sets were considered. Using the real Doppler blood flow signals, we also showed that it did not statistically matter whether the packets were dropped in uniform or random manners.

Acknowledgements

The study was supported by the Heinz Endowment Fund.

References

[1] I. D. Papel, *Facial Plastic and Reconstructive Surgery.* New York, NY: Thieme Medical Publishers, 2009.

[2] M. L. Urken, H. Weinberg, D. Buchbinder, J. F. Moscoso, W. Lawson, P. J. Catalano, and H. F. Biller, "Microvascular free flaps in head and neck reconstruction: report of 200 cases and review of complications," *Archives of Otolaryngology - Head and Neck Surgery*, vol. 120, no. 6, p. 633, Jun. 1994.

[3] G. D. Rosson, M. Magarakis, S. M. Shridharani, S. M. Stapleton, L. K. Jacobs, M. A. Manahan, and J. I. Flores, "A review of the surgical management of breast cancer: plastic reconstructive techniques and timing implications," *Annals of Surgical Oncology*, vol. 17, no. 7, pp. 1890–1900, Jul. 2010.

[4] B. Strauch and H.-L. Yu, *Atlas of microvascular surgery: Anatomy and operative approaches.* Thieme, 2006.

[5] S. Tamai, M. Usui, and T. Yoshizu, *Experimental and Clinical Reconstructive Microsurgery.* Springer, 2003.

[6] W. M. Swartz and J. C. Banis Jr, "Head and neck microsurgery," *Journal of Craniofacial Surgery*, vol. 3, no. 2, pp. 119–120, Sep. 1992.

[7] K. Z. Paydar, S. L. Hansen, D. S. Chang, W. Y. Hoffman, and P. Leon, "Implantable venous Doppler monitoring in head and neck free flap reconstruction increases the salvage rate," *Plastic and Reconstructive Surgery*, vol. 125, no. 4, pp. 1129–1134, Apr. 2010.

[8] D. Novakovic, R. S. Patel, D. P. Goldstein, and P. J. Gullane, "Salvage of failed free flaps used in head and neck reconstruction," *Head and Neck Oncology*, vol. 1, no. 1, pp. 33–1–5, Jul. 2009.

[9] G. M. Kind, R. F. Buntic, G. M. Buncke, T. M. Cooper, P. P. Siko, and H. J. Buncke Jr, "The effect of an implantable Doppler probe on the salvage of microvascular tissue transplants," *Plastic and Reconstructive Surgery*, vol. 101, no. 5, pp. 1268–1273, Apr. 1998.

[10] W. M. Swartz, R. Izquierdo, and M. J. Miller, "Implantable venous Doppler microvascular monitoring: Laboratory investigation and clinical results," *Plastic and Reconstructive Surgery*, vol. 93, no. 1, pp. 152–163, Jan. 1994.

[11] R. E. H. Ferguson Jr and P. Yu, "Techniques of monitoring buried fasciocutaneous free flaps," *Plastic and Reconstructive Surgery*, vol. 123, no. 2, pp. 525–532, Feb. 2009.

[12] B. C. Cho, D. P. Shin, J. S. Byun, J. W. Park, and B. S. Baik, "Monitoring flap for buried free tissue transfer: its importance and reliability," *Plastic and Reconstructive Surgery*, vol. 110, no. 5, pp. 1249–1258, Oct. 2002.

[13] J. J. Rosenberg, B. D. Fornage, and P. M. Chevray, "Monitoring buried free flaps: limitations of the implantable Doppler and use of color duplex sonography as a confirmatory test," *Plastic and Reconstructive Surgery*, vol. 118, no. 1, pp. 109–113, Jul. 2006.

[14] S. G. Pryor, E. J. Moore, and J. L. Kasperbauer, "Implantable Doppler flow system: Experience with 24 microvascular free-flap operations," *Otolaryngology - Head and Neck Surgery*, vol. 135, no. 5, pp. 714–718, Nov. 2006.

[15] B. Razavi, *RF Microelectronics*, ser. Prentice Hall International Series in the Physical and Chemical Engineering Sciences. Pearson Education, 2011.

[16] L. Couch, *Digital and Analog Communication Systems*. Pearson Education, 2012.

[17] E. Sejdić, M. Luccini, S. Primak, K. Baddour, and T. Willink, "Channel estimation using DPSS based frames," in *IEEE International Conference on Acoustics, Speech and Signal Processing (ICASSP 2008)*, Las Vegas, Nevada, USA, Mar./Apr. 31–4, 2008, pp. 2849–2852.

[18] E. Sejdić, A. Can, L. F. Chaparro, C. M. Steele, and T. Chau, "Compressive sampling of swallowing accelerometry signals using time-frequency dictionaries based on modulated discrete prolate spheroidal sequences," *EURASIP Journal on Advances in Signal Processing*, vol. 2012, pp. 101–1–14, May 2012.

[19] J. Oh, S. Senay, and L. F. Chaparro, "Signal reconstruction from nonuniformly spaced samples using evolutionary Slepian transform-based POCS," *EURASIP Journal on Advances in Signal Processing*, vol. 2010, 2010, article ID 367317, 12 pages.

[20] M. A. Davenport and M. B. Wakin, "Reconstruction and cancellation of sampled multiband signals using discrete prolate spheroidal sequences," in *Proc. of Workshop on Signal Processing with Adaptive Sparse Structured Representations (SPARS11)*, Edinburgh, Scotland, UK, Jun. 27-30, 2011, p. 61.

[21] J.-B. Lund, *Design Note DN502 CRC Implementation*, Texas Instruments, 2009. [Online]. Available: http://www.ti.com/lit/an/swra111d/swra111d.pdf

[22] *Low-Power SoC (System-on-Chip) with MCU, Memory, Sub-1 GHz RF Transceiver, and USB Controller*, Texas Instruments, 2013, pages 195-196. [Online]. Available: http://www.ti.com/lit/ds/swrs033h/swrs033h.pdf

[23] *Low-Power SoC (System-on-Chip) with MCU, Memory, Sub-1 GHz RF Transceiver, and USB Controller*, 2013, page 196. [Online]. Available: http://www.ti.com/lit/ds/swrs033h/swrs033h.pdf

[24] W. Dai and O. Milenković, "Subspace pursuit for compressive sensing signal reconstruction," *IEEE Transaction on Information Theory*, vol. 55, no. 5, pp. 2230–2249, May 2009.

[25] D. L. Donoho, "Compressed sensing," *IEEE Transactions on Information Theory*, vol. 52, no. 4, pp. 1289–1306, Apr. 2006.

[26] K.-K. Poh and P. Marziliano, "Compressive sampling of EEG signals with finite rate of innovation," *EURASIP Journal on Advances in Signal Processing*, vol. 2010, p. 12 pages, 2010, article ID 183105.

[27] E. J. Candes and M. B. Wakin, "An introduction to compressive sampling," *IEEE Signal Processing Magazine*, vol. 25, no. 2, pp. 21–30, Mar. 2008.

[28] S. Stanković, I. Orović, and E. Sejdić, *Multimedia Signals and Systems*. New York, NY: Springer US, 2012.

[29] H. Rauhut, K. Schnass, and P. Vandergheynst, "Compressed sensing and redundant dictionaries," *IEEE Transactions on Information Theory*, vol. 54, no. 5, pp. 2210 –2219, May 2008.

[30] E. J. Candés, J. Romberg, and T. Tao, "Robust uncertainty principles: Exact signal reconstruction from highly incomplete frequency information," *IEEE Transaction on Information Theory*, vol. 52, no. 2, pp. 489–509, Feb. 2006.

[31] E. Candés, J. K. Romberg, and T. Tao, "Stable signal recovery from incomplete and inaccurate measurements," *Communications on Pure and Applied Mathematics*, vol. 59, no. 8, pp. 1207–1223, Aug. 2006.

[32] E. Sejdić and L. F. Chaparro, "Recovering heart sounds from sparse samples," in *Proc. of 38th Annual Northeast Bioengineering Conference (NEBEC 2012)*, Philadelphia, PA, USA, Mar. 16–18, 2012, pp. 107–108.

[33] ——, "Time-frequency representations based on compressive samples," in *Proc. of 21st European Signal Processing Conference (EUSIPCO'13)*, Marrakech, Morocco, Sep. 9–13, 2013, pp. 1 569 742 057–1–4.

[34] H. B. Mann and D. R. Whitney, "On a test of whether one of two random variables is stochastically larger than the other," *The Annals of Mathematical Statistics*, vol. 18, no. 1, pp. 50–60, Mar. 1947.

[35] W. H. Kruskal and W. A. Wallis, "Use of ranks in one-criterion analysis of variance," *Journal of the American Statistical Association*, vol. 47, no. 260, pp. 583–621, Dec. 1952.

[36] L. Y. L. Mo and R. S. C. Cobbold, "A nonstationary signal simulation model for continuous wave and pulsed Doppler ultrasound," *IEEE Transactions on Ultrasonics, Ferroelectrics and Frequency Control*, vol. 36, no. 5, pp. 522–530, Sep. 1989.

[37] B. Boucheham, Y. Ferdi, and M. C. Batouche, "Recursive versus sequential multiple error measures reduction: A curve simplification approach to ECG data compression," *Computer Methods and Programs in Biomedicine*, vol. 81, no. 2, pp. 162–173, Feb. 2006.

[38] F. Scholkmann, S. Spichtig, T. Muehlemann, and M. Wolf, "How to detect and reduce movement artifacts in near-infrared imaging using moving standard deviation and spline interpolation," *Physiological Measurement*, vol. 31, no. 5, pp. 649–662, May 2010.